28 March 1996

PHYSICS LETTERS B

ELSEVIER

Physics Letters B 371 (1996) 175–180

Statistical multifragmentation in central Au + Au collisions at 35 MeV/u

M. D'Agostino [a], A.S. Botvina [b], P.M. Milazzo [c], M. Bruno [a], G.J. Kunde [d], D.R. Bowman [e], L. Celano [f], N. Colonna [f], J.D. Dinius [d], A. Ferrero [g], M.L. Fiandri [a], C.K. Gelbke [d], T. Glasmacher [d], F. Gramegna [h], D.O. Handzy [d], D. Horn [e], W.C. Hsi [d], M. Huang [d], I. Iori [g], M.A. Lisa [d], W.G. Lynch [d], L. Manduci [a], G.V. Margagliotti [c], P.F. Mastinu [a], I.N. Mishustin [i], C.P. Montoya [d], A. Moroni [g], G.F. Peaslee [d], F. Petruzzelli [g], L. Phair [d], R. Rui [c], C. Schwarz [d], M.B. Tsang [d], G. Vannini [c], C. Williams [d]

[a] *Dipartimento di Fisica and INFN, Bologna, Italy*
[b] *Hahn-Meitner-Institute, Berlin, Germany and Institute for Nuclear Research, Russian Academy of Science, 117312 Moscow, Russia*
[c] *Dipartimento di Fisica and INFN, Trieste, Italy*
[d] *NSCL, Michigan State University, USA*
[e] *Chalk River Laboratories, Chalk River, Canada*
[f] *INFN, Bari, Italy*
[g] *Dipartimento di Fisica and INFN, Milano, Italy*
[h] *INFN, Laboratori Nazionali di Legnaro, Italy*
[i] *Niels Bohr Institute, DK-2100 Copenhagen, Denmark and Kurchatov Institute, Russian Scientific Center, 123182 Moscow, Russia*

Received 29 November 1995; revised manuscript received 3 January 1996
Editor: C. Mahaux

Abstract

Multifragment disintegrations, measured for central Au + Au collisions at $E/A = 35$ MeV, are analyzed with the Statistical Multifragmentation Model. Charge distributions, mean fragment energies, and two-fragment correlation functions are well reproduced by the statistical breakup of a large, diluted and thermalized system slightly above the multifragmentation threshold.

Hot nuclear systems produced in intermediate energy nucleus-nucleus collisions are known to decay by multiple fragment emission [1–3]. While this decay mode may be related to a "liquid-gas" phase transition in finite nuclear systems, both statistical and dynamical aspects of multifragmenting finite nuclear systems must be understood before inferences about nuclear phase transitions can be made. Since the thermodynamic limit should be more readily reached for the heaviest possible nuclear systems, studies of central collisions between heavy nuclei, such as Au + Au, are of particular relevance.

Central collisions between heavy nuclei produce maximum fragment multiplicities at incident energies of $E/A \approx 100$ MeV [4,5]. Hot nuclear systems formed at this energy have, however, been shown to

Elsevier Science B.V.
PII S370-2693(96)00008-1

undergo a rapid collective expansion [6,7] which complicates a statistical interpretation of the decay [8,9]. The dynamics of collective expansion should be less important at lower incident energies [10,11] where comparisons with equilibrium statistical model calculations [1,3] should be more appropriate. In this paper we perform such a comparison for fragments produced in central Au + Au collisions at $E/A = 35$ MeV.

The experiment was performed at the National Superconducting Cyclotron Laboratory of the Michigan State University. Experimental details have already been reported in Refs. [10,11]. Briefly, charged particles of element number $Z \leq 20$ were detected at $23° \leq \theta_{lab} \leq 160°$ by 171 phoswich detector elements of the MSU Miniball array [12]; fragments with charge up to $Z = 83$ were detected at $3° \leq \theta_{lab} < 23°$ by the *Multics* array [13]. The geometric acceptance of the combined array was greater than 87% of 4π. The charge identification thresholds in the Miniball were $E_{th}/A \approx 2, 3, 4$ MeV for $Z = 3, 10, 18$, respectively, and $E_{th}/A \approx 1.5$ MeV in the Multics array, independent of the fragment charge. For the present analysis, central collisions are selected by requiring observed charged particle multiplicities $N_c > 24$ (representing about 10% of the total reaction cross section [11]).

For central events, the fragment emission was found [10,11] compatible with a near-isotropic decay of a source consisting of more than 300 nucleons and with negligible contributions from the decay of projectile and target-like residues. Here we address the question to which degree fragment emission can be described by a statistical equilibrium calculation performed with the Statistical Multifragmentation Model (SMM) of Refs. [3,14]. This model was successfully applied at higher energies to the interpretation of Au-induced projectile fragmentation reactions [15] for which collective expansion velocity components have been shown to be negligible and also for central collisions [16] for which the model has to be modified to take into account the large observed expansion velocities.

The model is based upon the assumption of statistical equilibrium at a low-density freeze-out stage of the reaction at which the primary fragments are formed according to their equilibrium partitions. The equilibrium partitions are calculated according to the micro-canonical ensemble of all break-up channels composed of nucleons and excited fragments of different masses [16]. The model conserves total excitation energy, momentum, mass and charge number. The statistical weight of decay channel j is given by $W_j \propto \exp S_j(E_s^*, A_s, Z_s)$, where S_j is the entropy of the system in channel j and E_s^*, A_s, and Z_s are the excitation energy, mass and charge number of the source. Different breakup configurations are initialized according to their statistical weights. The fragments are then propagated in their mutual Coulomb field and allowed to undergo secondary decays. Light fragments with mass number $A_f \leq 4$ are considered as stable particles ("nuclear gas") with only translational degrees of freedom; fragments with $A_f > 4$ are treated as heated nuclear liquid drops. The secondary decay of large fragments ($A_f > 16$) is calculated from an evaporation-fission model, and that of smaller fragments from a Fermi break-up model [14]. The simulated events were then filtered with the acceptance of the experimental apparatus [11,17]. The same normalization to the total number of events was applied to the experimental and calculated distributions, which thus may be compared on an absolute scale.

In its original version [14], the SMM only incorporates thermal degrees of freedom, i.e. the fragment energy distribution was determined from the source temperature and then modified by final-state Coulomb interactions and secondary decays. In the present work, we also allow for a collective radial expansion of the system which could arise from a rapid thermal expansion, possibly aided by an initial compression. Specifically, we assume that modest collective velocity components do not influence the fragment formation probabilities for a given thermal energy; this assumption is reasonable for $E_{flow}/A \leq 3$ MeV [3]. A self-similar collective expansion was assumed, $v_{flow} \propto r$, where r is the distance from the source's center of mass. This collective velocity was added to the thermal fragment velocity. The energy balance was taken into account.

In order to obtain an equilibrium freeze-out condition, we need to estimate mass, charge, and energy carried away by particles of early emission. For this purpose, we assume that the preequilibrium emission consists primarily of $n, p, d, t, {}^3\mathrm{He}$ and α-particles distributed uniformly in the available phase space in centre-of-mass system. Following Ref. [3], we search for parameters (mass A_s, charge Z_s, excitation en-

ergy E_s^*, and freeze-out density ρ_s, assuming $Z_s/A_s = 79/197$) of thermalized sources which can reproduce the experimental data.

To this aim we performed several calculations, varying in a wide range the input parameters. For each set the model provides a point in the $[N_c - N_{\rm IMF}]$ plane (where $N_{\rm IMF}$ is the multiplicity of the Intermediate Mass Fragments with charge $3 \leq Z \leq 30$), so it is possible to build a "net" around the experimental correlations [3] and to perform a rough estimate of the ranges of Z_s and E_s^*/A. The flow energy $E_{\rm flow}/A$ can approximatively determined by comparing the kinetic energy of fragments emitted around 90°, following Ref. [9].

To explore sensitivities to the assumed freeze-out density, we performed calculations for $\rho_s = \rho_0/3$ and $\rho_0/6$ (where $\rho_0 \approx 0.15$ fm^{-3} is the density of normal nuclear matter). A decrease of ρ_s to values smaller than $\rho_0/6$ would lead to an unrealistic increase of the flow energy, while ρ_s larger than $\rho_0/3$ would not satisfy the requirement of nonoverlapping primary fragments.

Improved source parameters can be obtained by analyzing the inclusive charge distribution $N(Z) = {\rm Yield}(Z)/N_{\rm events}$ (Figs. 1 a,b). Indeed, as shown in the following, the charge distribution at high values of the fragment charge fixes in a narrower range the thermal excitation energy. Moreover the comparison of $N(Z)$ in the whole Z-range allows to check the contemporary reproduction of the previously mentioned multiplicities, together with other observables, since $N_c = \int_1^{\infty} N(Z)\, dZ$, $N_{\rm IMF} = \int_3^{30} N(Z)\, dZ$), and $Z_{\rm tot} = \int_1^{\infty} N(Z) \cdot Z\, dZ$, where $Z_{\rm tot}$ is the total detected charge. In addition the comparison of the charge distribution of the heaviest fragments (Fig. 2) allows to check the reproduction of the event charge partition.

The flow energy can be more precisely determined by comparing more exclusive observables, such as the kinetic energy as a function of the emission angle, for each selected value of the fragment charge. The two-fragment correlation functions can be then used as a final test of the set of input parameters.

From the comparison of measured and predicted N_c, $N_{\rm IMF}$ it resulted that for $\rho_s = \rho_0/3$ the model can reproduce central collision data for $Z_s \approx (0.8 - 0.9) Z_{\rm tot}$ and $E_s^* \approx (0.6 - 0.7) E_{\rm tot}$ where $Z_{\rm tot}$ and $E_{\rm tot}$ denote the total available charge and center-of-mass

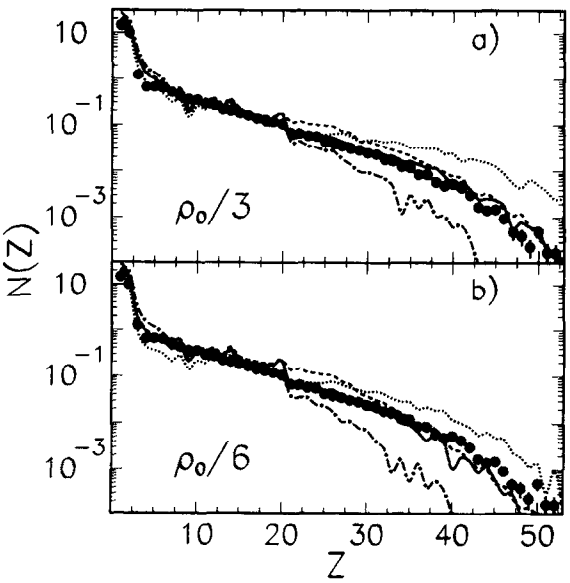

Fig. 1. Charge distribution $N(Z)$. Points show experimental data and lines show results of SMM predictions for sources with parameters $A_s = 343$, $Z_s = 138$, $E_s^*/A = 6.0$ MeV, $\rho_s = \rho_0/3$ (part a)) and $A_s = 315$, $Z_s = 126$, $E_s^*/A = 4.8$ MeV, $E_{\rm flow}/A = 0.8$ MeV, $\rho_s = \rho_0/6$ (part b)). Dashed curves are the unfiltered calculations and solid curves are the filtered ones. The dot-dashed and dotted curves represent filtered calculations for thermal excitations $E_s^*/A + 1$ MeV/u and $E_s^*/A - 1$ MeV/u, respectively.

energy. For $\rho_s = \rho_0/6$, the source parameters are about 10% smaller. By comparing the kinetic energies of fragments emitted at $\sim 90°$ the flow energy $E_{\rm flow}/A$ resulted 0 for $\rho_s = \rho_0/3$ and smaller than ~ 2 MeV for $\rho_s = \rho_0/6$. The approximate temperature and entropy per nucleon of the extracted sources are $T \approx 6$ MeV and $S/A \approx 1.5 - 1.6$ in both cases.

One can readily understand why sources of different excitation energy and density can produce similar fragment distributions. A system of lower density has smaller Coulomb barriers for fragment formation and thus requires a smaller temperature to break up into fragments. During the expansion to a lower density additional particles will be lost and some of the internal energy may be converted into radial flow. Therefore, the low-density source should have less mass and excitation energy.

We show hereafter SMM calculations for the two sets of source parameters, which resulted the best sets obtained with the previously outlined procedure:

$A_s = 343$, $Z_s = 138$, $E_s^*/A = 6.0$ MeV, $\rho_s = \rho_0/3$,
$A_s = 315$, $Z_s = 126$, $E_s^*/A = 4.8$ MeV, $\rho_s = \rho_0/6$.

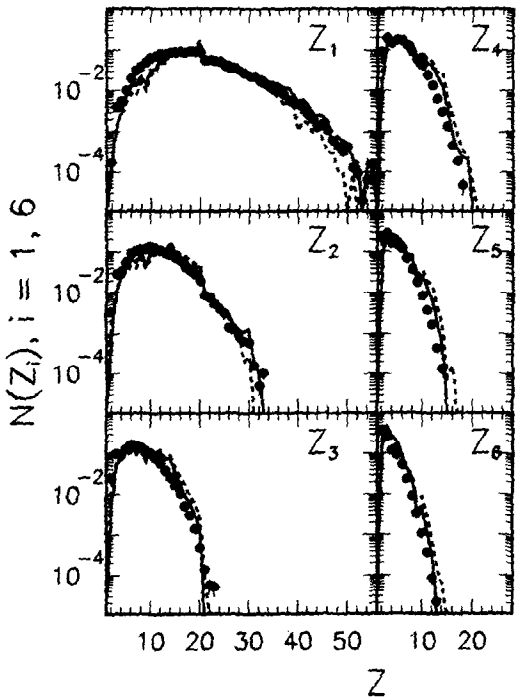

Fig. 2. Charge distribution of the six heaviest fragments, ordered such as $Z_i \geq Z_k$ if $i < k$. Experimental data are shown by points, the solid and dashed curves show the results of SMM calculations for $\rho_s = \rho_0/3$, and $\rho_s = \rho_0/6$, respectively (other source parameters as in Fig. 1).

In the second case an additional radial flow energy $E_{\text{flow}}/A = 0.8$ MeV was introduced (the total energy of the source was thus $E_s/A = 5.6$ MeV). This modest amount of radial flow is in agreement with the extrapolation of data at higher energies to $E/A = 35$ MeV [18]. As shown below, both sets of calculations reproduce the measured observables, both qualitatively and in absolute magnitude.

We have also considered a collective rotational motion with the same energy per nucleon as the flow energy and we found our main conclusions to be essentially unchanged as compared to the case of collective expansion.

In Fig. 1, the sensitivity to the excitation energy is illustrated by additional calculations performed for $E_s^*/A \pm 1$ MeV *per nucleon* (dot-dashed and dotted curves). From this figure it can be seen that the reproduction of $N(Z)$ at high values of the fragment charge allows for an unambiguous determination of the thermal excitation energy and the reproduction over several order of magnitude of the event charge partition,

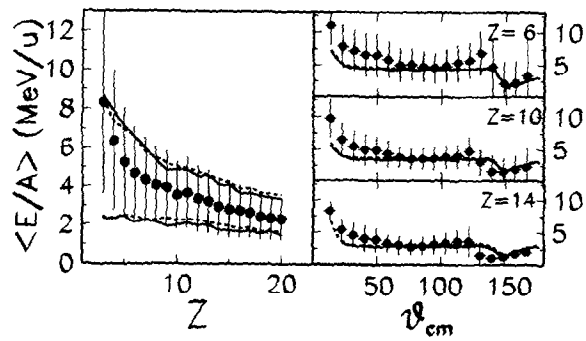

Fig. 3. Mean centre-of-mass kinetic energy per nucleon, $\langle E/A \rangle$, as a function of the charge Z, for fragments emitted at $\theta_{\text{cm}} = 90° \pm 10°$ (left panel) and (for $Z = 6, 10, 14$) as a function of θ_{cm} (right panels). Points give the experimental values of $\langle E/A \rangle$ and vertical bars give the standard deviations $\Delta E/A$ of the distributions. The solid and dashed lines are SMM predictions of $\langle E/A \rangle$ (in the left panel show the two values $\langle E/A \rangle \pm \Delta E/A$) for $\rho_s = \rho_0/3$, and $\rho_s = \rho_0/6$, respectively (other source parameters as in Fig. 1). The energy range is the same in the left and in each right panel.

represented in Fig. 2 trough the distribution of the six heaviest fragments (ordered according to $Z_i \geq Z_k$ if $i < k$).

A comparison of filtered and unfiltered calculations (solid and dashed curves, respectively) shows that distortions of the Z-distribution from to the experimental apparatus are relatively small, except in the region $Z > 20$ where the Miniball detectors lose charge resolution. In the region of large Z, the charge distribution falls off more steeply than expected for exponential or power-law distributions. This steep fall-off, reproduced in the calculations, is an effect of charge (mass) conservation for a finite system.

Mean values, $\langle E/A \rangle$ (solid points), and standard deviations $\Delta E/A$ (vertical bars) of the kinetic energies per nucleon of fragments emitted at $\theta_{\text{cm}} = 90° \pm 10°$ are shown in Fig. 3 (left panel) as a function of Z. The solid and dashed curves show the results of SMM calculations at $\langle E/A \rangle \pm \Delta E/A$ for $\rho_s = \rho_0/3$ and $\rho_0/6$, respectively, filtered by the acceptance of the experimental apparatus. Right panels of the figure show the dependence of $\langle E/A \rangle$ on θ_{cm} for $Z = 6, 10$, and 14. (The small rise in $\langle E/A \rangle$ at forward angles and the small dip at backward angles are caused by the acceptance of the experimental apparatus [11].) Overall, both SMM calculations reproduce the data rather well – the smaller Coulomb repulsion from the lower-density source is compensated by the added collective

expansion energy. Both calculations underpredict the kinetic energies of lighter fragments ($Z < 5$) and of fragments emitted at forward angles, possibly due to the presence of some nonequilibrium fragment emission in the data. The bulk of the data is, however, consistent with near-equilibrium emission from a single source [11].

In order to test the predicted spatial separation of emitted fragments, we have constructed two-fragment correlation functions [19],

$$1 + R(v_{\mathrm{red}}) = C\frac{Y(v_{\mathrm{red}})}{Y_{\mathrm{back}}(v_{\mathrm{red}})}$$

where

$$v_{\mathrm{red}} = \frac{|\,\boldsymbol{v}_i - \boldsymbol{v}_j\,|}{\sqrt{Z_i + Z_j}}$$

is the "reduced" relative velocity of fragments i and j ($i \neq j$) with charges Z_i and Z_j; $Y(v_{\mathrm{red}})$ and $Y_{\mathrm{back}}(v_{\mathrm{red}})$ are the coincidence and background yields for fragment pairs of reduced velocity v_{red} and $C = N_{\mathrm{back}}/N_{\mathrm{coinc}}$, where N_{coinc} and N_{back} are the total number of coincidence and background pairs. The background yield was constructed by means of the mixed event techniques [20,21].

Because of the large differences in dynamic range and resolution between the Multics and Miniball arrays, we separately evaluated the two-fragment correlation functions measured with the two devices. Figs. 4 a, b show, respectively, two-fragment correlations constructed solely from fragments detected in the Multics array ($3 \leq Z \leq 30$, $8° \leq \theta_{\mathrm{lab}} < 23°$) and in the Miniball ($3 \leq Z \leq 10$, $23° \leq \theta_{\mathrm{lab}} \leq 40°$). The solid and dashed curves show the results of SMM calculations performed for $\rho_s = \rho_0/3$ and $\rho_0/6$, respectively, filtered for the acceptance of the experimental apparatus. Overall, the measured correlation functions are approximately reproduced by the calculations. Some discrepancies may be caused by the small differences found in the event charge partitions shown in Fig. 2 (see analysis on Ref. [22]). The increased overshoot just after the *Coulomb hole* for the case $\rho_s = \rho_0/6$ is caused by the flow: more "organized" motion produces additional correlations in single events.

Two-fragment correlation functions measured in this experiment are also reproduced [11] by assuming sequential emission from the surface of a spherical

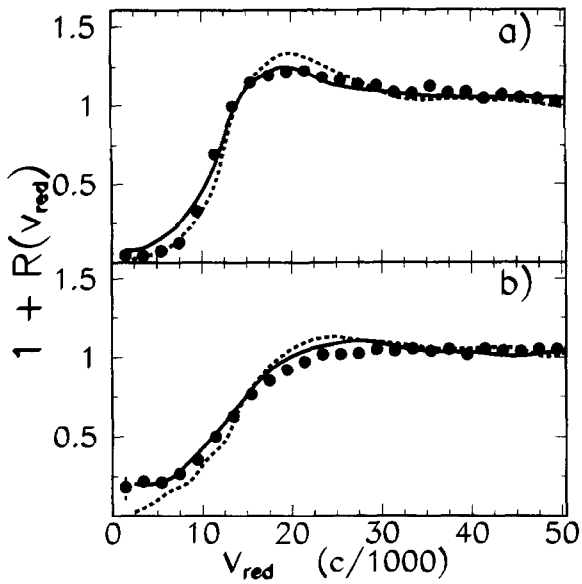

Fig. 4. Two-fragment correlation functions $1 + R(v_{\mathrm{red}})$ for $3 \leq Z \leq 30$ and $8° \leq \theta_{\mathrm{lab}} < 23°$ (part a)) and for $3 \leq Z \leq 10$ and $23° \leq \theta_{\mathrm{lab}} \leq 40°$ (part b)). Full points show experimental data. The solid and dashed lines are SMM predictions for $\rho_s = \rho_0/3$, and $\rho_s = \rho_0/6$ (other source parameters as in Fig. 1).

source of charge $Z_s = 138$, breakup density $\rho_s = \rho_0/4$, radial expansion velocity $v_{\mathrm{flow}} = 1.4$ cm/ns and average interfragment emission time $\tau \approx 85$ fm/c. Since in the SMM we increase effectively the time of fragment production (and decrease the initial correlation) by including the secondary de-excitation, we can consider these results in agreement with the present analysis. Moreover, this ambiguity in interpretation could be ascribed to the fact that the angle integrated correlation functions are affected by both the source's size and its lifetime, resulting in the well known space-time ambiguity [19,23]. In favorable situations [23–25], this ambiguity could be reduced by studying detailed energy and angle dependences of the two-fragment correlation functions.

The source parameters extracted in our analysis are also consistent with expectation from dynamical simulations. We have performed such simulations with the Boltzmann-Nordheim-Vlasov (BNV) model [26] for central collisions ($b \leq 1$ fm) using the mean-field approximation with a soft equation of state. Approximately 100 fm/c after the initial contact between projectile and target, the calculations predict the formation of a single source of mass $A \approx 324$, charge $Z \approx$

136, density $\rho = \rho_0/2$, excitation energy per nucleon $E^*/A \approx 6$ MeV, and rotational energy $E_{rot} \approx 10$ MeV. Unfortunately, BNV-type models do not treat emission of single fragments.

In conclusion, fragment emission observed in central Au + Au collisions at $E/A = 35$ MeV is largely consistent with the statistical break-up of a single source of excitation energy per nucleon $E_s^*/A \approx 5$–6 MeV and density $\rho_s = \rho_0/3$–$\rho_0/6$. Collective expansion energy is not excluded but it is smaller than ~ 1 MeV/u. These conditions are comparable to those observed for peripheral projectile fragmentation reactions at higher energies ($E/A > 400$ MeV). However, these reactions can only produce smaller sources of mass and charge numbers $A_s < A_{projectile}$ and $Z_s < Z_{projectile}$.

The authors would like to thank A. Bonasera and M. Di Toro for many interesting and stimulating discussions and for making their codes available. The technical assistance of R. Bassini, C. Boiano, S. Brambilla, G. Busacchi, A. Cortesi, M. Malatesta and R. Scardaoni during the measurements is gratefully acknowledged. This work has been supported in part by funds of the Italian Ministry of University and Scientific Research and by the US National Science Foundation under Grant number PHY-92-14992. A.S. Botvina thanks the Hahn-Meitner Institute for hospitality and support, I.N. Mishustin thanks the Niels Bohr Institute for hospitality and Carlsberg Foundation (Denmark) for financial support.

References

[1] D.H.E. Gross, Rep. Progr. Phys. 53 (1990) 605.
[2] L.G. Moretto and G.J. Wozniak, Ann. Rev. Nucl. Part. Sci. 43 (1993) 379, and references quoted therein.
[3] J.P. Bondorf, A.S. Botvina, A.S. Iljinov, I.N. Mishustin and K. Sneppen, Phys. Rep. 257 (1995) 133.
[4] M.B. Tsang et al., Phys. Rev. Lett. 71 (1993) 1502.
[5] G.F. Peaslee et al., Phys. Rev. C 49 (1994) R2271.
[6] S.C. Jeong et al., Phys. Rev. Lett. 72 (1994) 3468.
[7] W.C. Hsi et al., Phys. Rev. Lett. 73 (1994) 3367.
[8] B. Heide and H.W. Barz, Nucl. Phys. A 588 (1995) 918.
[9] G.J. Kunde et al., Phys. Rev. Lett. 74 (1995) 38.
[10] M. D'Agostino et al., Phys. Rev. Lett. 75 (1995) 4373.
[11] M. D'Agostino et al., Phys. Lett. (1995), in press.
[12] R.T. DeSouza et al., Nucl. Instr. and Meth. A 295 (1990) 109.
[13] I. Iori et al., Nucl. Instr. and Meth. A 325 (1993) 458; M. Bruno et al., Nucl. Instr. and Meth. A 311 (1992) 189; N. Colonna et al., Nucl. Instr. and Meth. A 321 (1992) 529; P.F. Mastinu et al. Nucl. Instr. and Meth. 338 (1994) 419.
[14] A.S. Botvina et al., Nucl. Phys. A 475 (1987) 663.
[15] A.S. Botvina et al., Nucl. Phys. A 584 (1995) 737.
[16] J.P. Bondorf, A.S. Botvina, I.N. Mishustin and S.R. Souza, Phys. Rev. Lett. 73 (1994) 628.
[17] M. Bruno et al., Nucl. Instr. and Meth. A 305 (1991) 410.
[18] W. Reisdorf et al., Proc. the Intern. Workshop XXII, Hirshegg 1994, Eds. H. Feldmeier and W. Nörenberg, p. 93.
[19] Y.D. Kim et al., Phys. Rev. C 45 (1992) 338, 387.
[20] R. Trockel et al., Phys. Rev. Lett. 59 (1987) 2844.
[21] M.A. Lisa et al., Phys. Rev. C 44 (1991) 2865.
[22] O. Schapiro and D.H.E. Gross, Nucl. Phys. A 573 (1994) 143, 428.
[23] T. Glasmacher et al., Phys. Rev. C 50 (1994) 952.
[24] T. Glasmacher, C.K. Gelbke and S. Pratt, Phys. Lett. B 314 (1993) 265.
[25] E. Cornell et al., Phys. Rev. Lett. 75 (1995) 1475.
[26] A. Bonasera et al., Phys. Lett. B 221 (1989) 233.